

# Thermal Atom-Ion Collisions in K-Yb<sup>+</sup> Hybrid System

Thai M. Hoang,<sup>1</sup> Peter D. D. Schwindt,<sup>1</sup> and Yuan-Yu Jau<sup>1</sup>

<sup>1</sup>*Sandia National Laboratories, Albuquerque, NM 87123, USA*

(Dated: November 30, 2023)

We report experimental studies of atom-ion collisions in a temperature range of several hundred Kelvin (thermal regime) using trapped ytterbium (Yb<sup>+</sup>) ions immersed in potassium (K) vapor. Various collisional rate coefficients of the Yb<sup>+</sup> ion per K-atom number density are measured. We find the isotopically dependent charge-exchange rate coefficients to be  $\kappa_{ce} = (12.7 \pm 0.8) \times 10^{-14} \text{ cm}^3 \text{ s}^{-1}$  and  $\kappa_{ce} = (5.3 \pm 0.3) \times 10^{-14} \text{ cm}^3 \text{ s}^{-1}$  for K-<sup>171</sup>Yb<sup>+</sup> and K-<sup>172</sup>Yb<sup>+</sup> respectively. The spin-destruction rate coefficient is  $\kappa_{sd} = (1.46 \pm 0.29) \times 10^{-9} \text{ cm}^3 \text{ s}^{-1}$ , and the spin-exchange rate coefficient is  $\kappa_{se} = (1.64 \pm 0.24) \times 10^{-9} \text{ cm}^3 \text{ s}^{-1}$ , which are isotopically independent. Unlike alkali-alkali atomic systems that normally have  $\kappa_{se} \gg \kappa_{sd}$ , this thermal K-Yb<sup>+</sup> system has  $\kappa_{se} \sim \kappa_{sd}$ , which is not fully understood with present theory. Similar results have also been reported previously from other cold atom-ion hybrid systems. It is important to investigate hybrid systems of different atom-ion species to achieve better understanding on the collisional physics for atom-ion based quantum applications.

While free thermal atoms, trapped neutral atoms, and trapped ions are well established platforms for atomic-physics research and applications, a hybrid system of neutral atoms and ions can offer new capabilities and opportunities that cannot be accomplished with only one atomic species. In 1960s and 1970s, the spin-dependent charge exchange between <sup>3</sup>He<sup>+</sup> ions and Cs atoms was utilized to measure the ground-state hyperfine splitting of <sup>3</sup>He<sup>+</sup> ions, because the narrow-band light source at 41-eV photon energy was too difficult to construct for directly probing the internal state of <sup>3</sup>He<sup>+</sup> [1, 2]. Up to date, this Cs mediated method still delivers the best result of the <sup>3</sup>He<sup>+</sup> hyperfine splitting frequency. In addition, the spin-exchange interactions between free ions and Rb atoms were used to study hyperfine spectroscopy of Sr<sup>+</sup>, Cd<sup>+</sup>, and Hg<sup>+</sup> ions [3, 4]. These atom-ion hybrid systems demonstrated a great potential for atomic metrology applications such as fieldable ion clocks[5], to eliminate the need of miniaturized, low-power, short-wavelength (blue to ultra violet, UV) lasers for interrogation of ion systems. Recently, a hybrid system of cold neutral atoms and cold ions has become an attractive platform to study quantum physics of heterosystems[6, 7], which will advance our knowledge in cold collisions, quantum chemistry, many-body physics, quantum simulation[6], and quantum computation[8].

In the past decades, various collisional phenomena in atom-ion systems have been investigated broadly in theoretical work (summarized in Ref.[6]); however, the experimental studies are limited [9–16]. More experimental research work will benefit the theoretical framework of ion-atom interactions. In this paper, we study the K-Yb<sup>+</sup> hybrid system using trapped ytterbium (Yb<sup>+</sup>) ions and free potassium (K) atoms (vapor). To our knowledge, there are no previously reported results of the K-Yb<sup>+</sup> system either in theory or experiments. Through our experiments, we determine the charge-exchange, spin-exchange, and spin-destruction rate coefficients for Yb<sup>+</sup> ions and K atoms. Ideally, if the collisions follow the Langevin

model[6], the rate coefficients are nearly independent of the collisional kinetic energy. While the previous experimental studies using hybrid ion-atom systems were in the ultra-cold regime, our experiment is carried out in the thermal regime. This would help further understanding of the collisional interactions of hybrid systems in a wider temperature range.

Our experimental apparatus comprises a vacuum chamber for the atom-ion hybrid environment, B-field coils, and various laser sources. Inside the vacuum chamber, there is a linear Paul trap with four 50-mm long rods (6-mm apart along each side) and two hollow end caps, and there are two Yb sources (natural abundance and isotopically enriched) and one K getter (dispenser) source (natural abundance). The chamber was baked out to achieve 10<sup>-10</sup> torr level and then was back filled with 45 × 10<sup>-6</sup> torr of helium gas for buffer-gas cooling to the trapped Yb<sup>+</sup> ions. The K getter was driven by 2.5-A DC current during the bakeout to clean up the possible outgassing sources on the getter. The trap rods were driven by a 1.95-MHz RF source at 780 V<sub>pk-pk</sub> and the end caps were connected to a 15-V DC source. We trapped > 10<sup>6</sup> ions with an ion density on the order of 10<sup>8</sup> cm<sup>-3</sup> and the measured ion temperature  $T_{Yb^+} \approx 600 - 700$  K. The laser sources include 369-nm, 399-nm, and 935-nm lasers for ion loading, state preparation, and interrogation of Yb<sup>+</sup> ions[5, 17], and 766-nm and 770-nm lasers for optical pumping and probing of K atoms. As illustrated in Fig. 1a, the 369-nm laser is delivered to the ion cloud to provide state detection and optical pumping of the trapped ions, and the 935-nm laser clears the low-lying  $D_{3/2}$  state. Fluorescence at 369 nm or 297 nm is collected with a photon multiplier tube (PMT). To study the interactions between Yb<sup>+</sup> ion and K atoms, the vacuum chamber is filled with K vapor released from a potassium getter. The K vapor density is controlled through the electrical current applied on the getter. The measured K-atom temperature is  $T_K \approx 340$  K. A linearly polarized 770-nm laser beam with a doughnut profile is

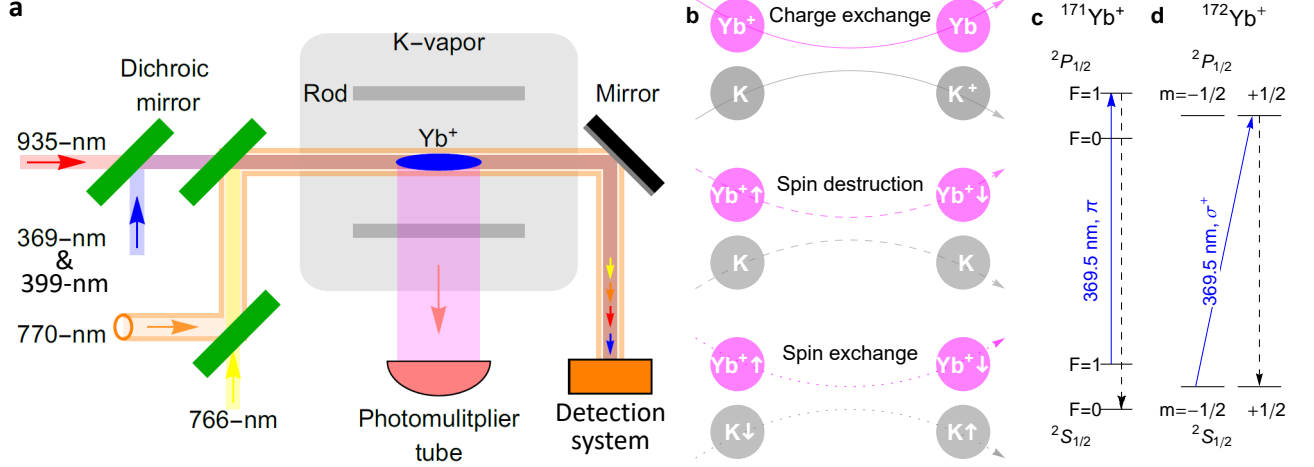
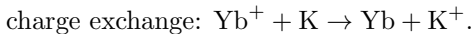


FIG. 1. a) The  $\text{Yb}^+$  ions cloud (blue) are trapped in a linear Paul trap. The 369-nm, 399-nm, 935-nm, 770-nm, and 766-nm laser beams are combined using dichroic mirrors. The fluorescence signal of the  $\text{Yb}^+$  ions is collected by a PMT. The laser beams go to a detection system with different wavelength filters. K atoms (gray area) are released into the chamber from a potassium getter. b) Illustrations of the charge-exchange, the spin-destruction, and the spin-exchange interactions. The up and down arrows represent an atomic spin. c) Hyperfine polarization of  $^{171}\text{Yb}^+$  ions achieved by optical pumping. d) Spin polarization of  $^{172}\text{Yb}^+$  ions achieved by optical pumping.

used as a probe to measure the K-vapor density and temperature. The same laser beam is used to optically spin-polarize K atoms with circular polarization. The dark center of the doughnut beam is aligned to the ion cloud axis. A linearly polarized 766-nm laser beam through the ion cloud is used for an optical rotation (Faraday effect) measurement[18, 19] to determine the degree of spin polarization of the K atoms inside the ion cloud. Both the number density and the temperature of the trapped  $\text{Yb}^+$  ions and K atoms can be determined by measuring the signal contrast and the Doppler profile of the optical resonances through scanning the frequency of the transmitting probe laser across the  $D1$  resonances[18, 19]. We used B-field coils to compensate the ambient magnetic field and set the preferred magnetic-field direction for the experiment.

Figure 1b illustrates different collisional interactions, such as charge exchange, spin destruction, and spin exchange. The charge-exchange interaction occurs when an electron migrates from a neutral K atom to a  $\text{Yb}^+$  ion during the collision (There could be an intermediate state  $(\text{YbK})^+$  during the collisional process.):



After charge-exchange collisions, the neutral Yb can no longer be trapped. This leads to the main ion loss mechanism. We can measure the charge-exchange induced ion-loss rate to determine the charge-exchange rate coefficient via the following relation:

$$\gamma_{\text{ce}} = \frac{1}{\tau_{\text{ce}}} = \kappa_{\text{ce}} \cdot n_{\text{K}}, \quad (1)$$

where  $\gamma_{\text{ce}}$  is the charge-exchange rate,  $\tau_{\text{ce}}$  is the exponential ion loss time constant,  $n_{\text{K}}$  is the number density of K atoms, and  $\kappa_{\text{ce}}$  is the charge-exchange rate coefficient. Here, the rate coefficient  $\kappa = \langle \sigma v \rangle$  is an ensemble average of all possible velocity-dependent cross section  $\sigma(v)$  and colliding relative velocity  $v$ .

To measure  $\tau_{\text{ce}}$ , we delivered a 1-mm diameter, 3-mW cw 935-nm laser beam overlapped with a 1-mm diameter 369-nm laser beam to the ion cloud. The 369-nm laser was at 1  $\mu\text{W}$ , pulsed every 11 minutes for 0.4 s.  $^{171}\text{Yb}^+$  ions are kept in the dark for 99.94% of time to eliminate any possible laser associated ion-signal-loss effects, such as F-state trapping[17] and laser-enhanced charge exchange (will be explained later). For  $^{172}\text{Yb}^+$ , we used a 0.2  $\mu\text{W}$  369-nm laser, 4-s pulsed repeated every 11 minutes for the same reasons. We carefully verified that the 369-nm laser power and its duty cycle were sufficiently low to make sure no noticeable effect to be seen from the presence of the 369-nm laser. The typical fluorescence signals of  $\text{Yb}^+$  ions are shown in Fig. 2a. To extract  $\tau_{\text{ce}}$ , we fit the data to an exponential function. The data indicates that the  $^{171}\text{Yb}^+$  ions leave the trap about twice faster than  $^{172}\text{Yb}^+$  ions with the same K-atom density. The summary of experimental data of  $1/\tau_{\text{ce}}$  for  $^{171}\text{Yb}^+$  and  $^{172}\text{Yb}^+$  with different K-atom density  $n_{\text{K}}$  are shown in Fig 2b. With linear fits, we find the charge-exchange rate coefficient to be

$$\begin{aligned} {}^{171}\kappa_{\text{ce}} &= (12.7 \pm 0.8) \times 10^{-14} \text{ cm}^3\text{s}^{-1} \\ {}^{172}\kappa_{\text{ce}} &= (5.3 \pm 0.3) \times 10^{-14} \text{ cm}^3\text{s}^{-1}. \end{aligned}$$

Since the charge-exchange efficiency is strongly related to the electronic structures of the two colliding species,

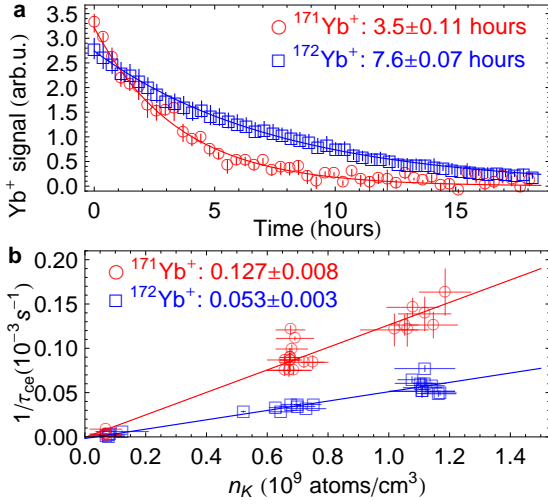


FIG. 2. a) Decay signals of  $\text{Yb}^+$  ions due to ion loss under the presence of  $\sim 7 \times 10^8 \text{ cm}^{-3}$  K-atom number density. The data are fitted to an exponential function to extract  $\tau_{\text{ce}}$ . The numbers represent the charge-exchange time constants and the fitting standard errors. b) The charge-exchange rate of a  $\text{Yb}^+$  ion under different potassium densities. Experimental data of  $^{171}\text{Yb}^+$  ( $^{172}\text{Yb}^+$ ) ions are shown in red (blue). The data are fitted to a linear function to extract  $\kappa_{\text{ce}}$ .

the different electronic energy-level structures of  $^{171}\text{Yb}^+$  and  $^{172}\text{Yb}^+$  ions may explain their significantly different rate coefficients. It is worth noting that the ion loss rate under the presence of K atoms increases rapidly when the  $\text{Yb}^+$  ions are exposed to  $D1$  resonant 369-nm laser, or the K atoms inside the ion cloud are exposed to  $D1$  resonant 770-nm laser. We believe this is caused by the much stronger charge-exchange interaction when the colliding ion or atom is in the excited state. Based on our experimental parameters, we estimated the charge-exchange rate coefficient to be on the order of  $10^{-9}$  to  $10^{-8} \text{ cm}^3\text{s}^{-1}$  if one of the colliding species is in its excited state ( $P_{1/2}$ ).

Atom-ion collisions can induce not only charge exchange but also spin flips, including random spin flips that destroy the spin polarization of the colliding atomic species, and spin exchange that swaps the electronic angular momentum between the ion and the atom. These spin-dependent collisional effects on the  $\text{Yb}^+$  ion leads to these forms:

$$\begin{aligned} \text{spin exchange: } & \text{Yb}^+ \uparrow + \text{K} \downarrow \rightarrow \text{Yb}^+ \downarrow + \text{K} \uparrow, \\ \text{spin destruction: } & \text{Yb}^+ \uparrow\downarrow + \text{K} \rightarrow \text{Yb}^+ \uparrow\downarrow + \text{K}. \end{aligned}$$

Here the  $\uparrow, \downarrow$  arrows represent the spin state. The dynamic of the  $\text{Yb}^+$  spin polarization is described by

$$\dot{P}_{\text{Yb}^+} = R_{\text{op}}(1 - P_{\text{Yb}^+}) + n_K [\kappa_{\text{se}}(P_K - P_{\text{Yb}^+}) - \kappa_{\text{sd}}P_{\text{Yb}^+}], \quad (2)$$

where  $R_{\text{op}}$  is the optical pumping rate on the ions,  $P_{\text{Yb}^+}$  and  $P_K$ , ranging from -1 to 1, are the spin polarization for the  $\text{Yb}^+$  ions and K atoms, and  $\kappa_{\text{sd}}$  and  $\kappa_{\text{se}}$  are

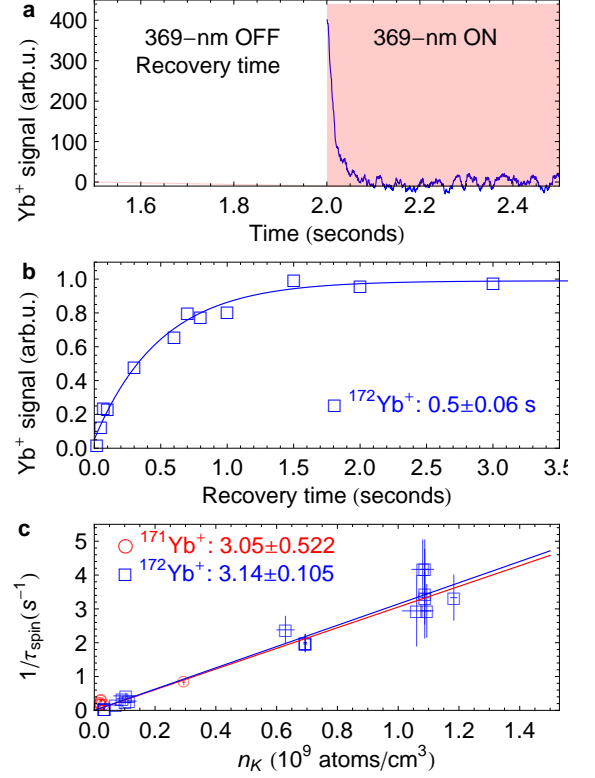


FIG. 3. a) The red shaded area represents the 50-nW, 0.5-s pulse of the circularly polarized 369-nm laser light. b) The data points represent the areas under of the fluorescence transient curves for different recovery time periods, where  $n_K \sim 7 \times 10^8 \text{ cm}^{-3}$ . The numbers represent the spin recovery time constants and the fitting standard errors. Each data point is an average of 200 runs. c) The spin recovery time constants versus different K number densities. Data of  $^{172}\text{Yb}^+$  ions and  $^{171}\text{Yb}^+$  ions are shown in blue markers and red markers, respectively. The  $^{171}\text{Yb}^+$  data uses similar procedure for  $^{172}\text{Yb}^+$  instead of the 369-nm laser is linearly polarized at 5  $\mu\text{W}$  with 3.5-s pulse width.

the rate coefficients for the spin-destruction and spin-exchange interactions. From Eq. 2, with  $R_{\text{op}} = 0$  and  $P_K = 0$ , we find the total spin-relaxation time constant to be  $\tau_{\text{spin}} = \gamma_{\text{spin}}^{-1} = [(\kappa_{\text{sd}} + \kappa_{\text{se}})n_K]^{-1}$ . To measure the total spin-relaxation rate  $\gamma_{\text{spin}}$ , we keep the K atoms unpolarized (i.e.  $P_K = 0$ ), and we spin-polarize the  $^{172}\text{Yb}^+$  ions by applying a circularly polarized 369-nm laser to pump the  $^{172}\text{Yb}^+$  ion into the  $|m = 1/2\rangle = |\uparrow\rangle$  or  $|m = -1/2\rangle = |\downarrow\rangle$  state in its Zeeman sublevels as illustrated in Fig. 1d. As shown in Fig. 3a, when the unpolarized  $^{172}\text{Yb}^+$  ions are illuminated by the 369-nm laser light, fluorescence appears at the beginning and then decays as most of the ions are spin polarized ( $P_{\text{Yb}^+} \sim 1$ ), where ions are in the dark state of the pump light and the photon scattering is minimized. During the “OFF” period of the pump light (i.e.  $R_{\text{op}} = 0$ ), the spin relaxation process reduces  $P_{\text{Yb}^+}$  and therefore recovers the fluorescence signal when the pump light turns on again.

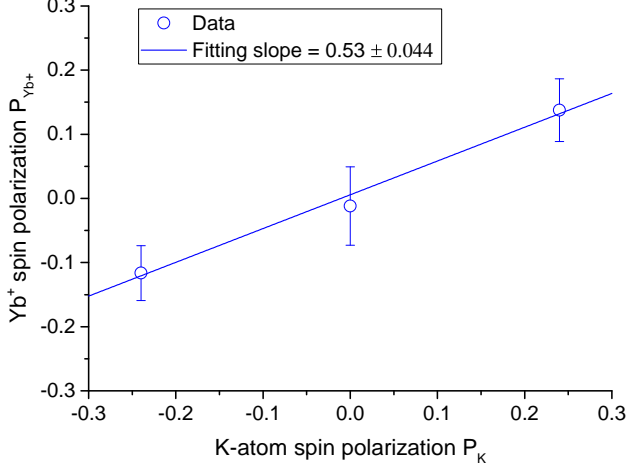


FIG. 4. Measured steady-state spin polarization of  $\text{Yb}^+$  ions versus K-atom spin polarization.

Figure 3b plots the signal strength as the "OFF" period (the recovery time) is varied, where the signal strength is the area under the transient curve of the fluorescence signal in Fig. 3a, which is proportional to the number of unpolarized ions. We determine  $\tau_{\text{spin}}$  (the recovery time constant) by an exponential fit to the data. By measuring the linear dependence of  $\gamma_{\text{spin}}$  on  $n_K$ , the total spin-relaxation rate coefficient ( $\kappa_{\text{sd}} + \kappa_{\text{se}}$ ) can be acquired. For the  $^{171}\text{Yb}^+$  ions, due to the optically resolved hyperfine splitting, the hyperfine optical pumping is easier to perform. The hyperfine polarization is achieved by pumping the ions into  $F = 0$  state as shown in Fig. 1c. With some detailed calculations[19], we find that we can use the same signal recovery measurement procedure to obtain ( $\kappa_{\text{sd}} + \kappa_{\text{se}}$ ). The experimental results are summarized in Fig. 3c, which gives a mean value of  $(\kappa_{\text{sd}} + \kappa_{\text{se}}) = (3.1 \pm 0.38) \times 10^{-9} \text{ cm}^3 \text{ s}^{-1}$  for both isotopes.

Based on Eq. 2, we can further determine  $\kappa_{\text{sd}}$  and  $\kappa_{\text{se}}$  separately by the steady-state value of  $P_{Yb^+}$  when  $R_{\text{op}} = 0$  through the following mathematical relation:

$$P_{Yb^+} = \frac{\kappa_{\text{se}} P_K}{\kappa_{\text{sd}} + \kappa_{\text{se}}} \quad (3)$$

To spin polarize the K atoms, we engaged a resonant 770-nm circularly polarized laser beam with a ring-shape profile at the ion cloud, so the ions can be fit inside the dark volume (5-cm long, > 2-mm diameter) of the doughnut profile to minimize the very large charge-exchange effect between the  $\text{Yb}^+$  ions and the excited K atoms. The doughnut beam was generated using a single-lens imaging technique. The doughnut profile has a bright ring about 1-mm wide and 6.4 mW total optical power. The 770-nm laser linewidth was intentionally broadened to about 1-GHz to match up the Doppler-profile of the K-atom  $D1$  resonance. The measured maximum positive

and negative K-atom spin polarization at the ion cloud inside the dark volume is  $\pm 0.24$  using the optical rotation method with a weak and optically detuned 766-nm beam. With these experimental conditions, Fig. 4 summarizes the results of  $P_{Yb^+}$  versus  $P_K$ , where  $P_{Yb^+}$  can be well calibrated by measuring the signal levels the ion fluorescence with conditions of  $P_{Yb^+} = 0$  and  $P_{Yb^+} = 1$ . Using Eq. 3, we find  $\kappa_{\text{se}} = (1.64 \pm 0.24) \times 10^{-9} \text{ cm}^3 \text{ s}^{-1}$ , and  $\kappa_{\text{sd}} = (1.46 \pm 0.29) \times 10^{-9} \text{ cm}^3 \text{ s}^{-1}$ . Since the K vapor density is controlled by the electric current through the K-getter (dispenser), one may wonder if some gas background was also produced when the K-getter temperature increased. Based on some previously reported spin-destruction cross section data[17], this would required the gas pressure to be  $\geq 10^{-5}$  torr to affect our spin-destruction measurements, which can be easily detected by the residual gas analyzer (RGA) in our vacuum system. But we found no detectable, additional gas background during the production of the K vapor.

With the relative collisional velocity  $\bar{v} = 4.6 \times 10^4 \text{ cm/s}$  determined by the temperatures of  $\text{Yb}^+$  ions and K atoms, we find the effective spin-exchange cross section  $\bar{\sigma}_{\text{se}} = \kappa_{\text{se}} / \bar{v} = 3.6 \times 10^{-14} \text{ cm}^2$ , which is similar to that of many alkali-alkali pairs[19] in the thermal regime. For most applications using the atom-ion hybrid platform,  $\kappa_{\text{se}} \gg \kappa_{\text{sd}}$  and  $\kappa_{\text{se}} \gg \kappa_{\text{ce}}$  will be the preferred conditions[20]. Under these conditions, the interactions of the quantum states between the neutral atom and the ion via spin-exchange would be stronger than the decoherence mechanism due to spin destruction, and atoms and ions would not change their original forms via charge exchange for sufficiently long period. A recent cold Rb- $\text{Yb}^+$  experiment[14] and this thermal K- $\text{Yb}^+$  work have both shown  $\kappa_{\text{se}} \sim \kappa_{\text{sd}}$ . The cold regime results may be explained by the theoretical work of Tscherbul *et al.* [21]. But there is still no good theoretical explanation for thermal regime. The relatively large  $\kappa_{\text{sd}}$  may be understood by further detailed modeling of the spin-orbit interactions[21, 22] in the future. In conclusion, we have studied the collisional effects in a thermal K- $\text{Yb}^+$  system. Our work may provide further insight to help establish ion clocks that do not use a UV light source and help study the quantum physics of atom-ion hybrid platforms.

We would like to thank Mr. Jeff Hunker for his help on setting up the experimental apparatus. This research was performed with funding from the Defense Advanced Research Projects Agency (DARPA). The views, opinions and/or findings expressed are those of the author and should not be interpreted as representing the official views or policies of the Department of Defense or the U.S. Government. Sandia National Laboratories is a multi-mission laboratory managed and operated by National Technology and Engineering Solutions of Sandia, LLC, a wholly owned subsidiary of Honeywell International, Inc., for the U.S. Department of Energys National Nuclear Security Administration under contract DE-NA0003525.

- 
- [1] E. Fortson, F. Major, and H. Dehmelt, Phys. Rev. Lett. **16**, 221 (1966).
  - [2] H. Schuessler, E. Fortson, and H. Dehmelt, Phys. Rev. **187**, 5 (1969).
  - [3] H. Gibbs and G. Churchill, Phys. Rev. A **3**, 1617 (1971).
  - [4] H. Schuessler and S. Hoverson, Phys. Lett. A **43**, 25 (1973).
  - [5] Y.-Y. Jau, H. Partner, P. D. D. Schwindt, J. D. Prestage, J. R. Kelloff, and N. Yu, Appl. Phys. Lett. **101**, 253518 (2012).
  - [6] M. Tomza, K. Jachymski, R. Gerritsma, A. Negretti, T. Calarco, Z. Idziaszek, and P. S. Julienne, arXiv preprint arXiv:1708.07832 (2017).
  - [7] H. A. Frst, N. V. Ewald, T. Secker, J. Joger, T. Feldker, and R. Gerritsma, J. Phys. B: Atomic, Molecular and Optical Physics **51**, 195001 (2018).
  - [8] H. Doerk, Z. Idziaszek, and T. Calarco, Phys. Rev. A **81**, 012708 (2010).
  - [9] J. L. Winthrop W. Smith, Oleg P. Makarov, J. Mod. Opt. **52**, 2253 (2005).
  - [10] A. T. Grier, M. Cetina, F. Oručević, and V. Vuletić, Phys. Rev. Lett. **102**, 223201 (2009).
  - [11] C. Zipkes, S. Palzer, L. Ratschbacher, C. Sias, and M. Köhl, Phys. Rev. Lett. **105**, 133201 (2010).
  - [12] C. Zipkes, S. Palzer, C. Sias, and M. Köhl, Nature **464**, 388 (2010).
  - [13] S. Schmid, A. Härter, and J. H. Denschlag, Phys. Rev. Lett. **105**, 133202 (2010).
  - [14] L. Ratschbacher, C. Sias, L. Carcagni, J. M. Silver, C. Zipkes, and M. Kohl, Phys. Rev. Lett. **110**, 160402 (2013).
  - [15] W. W. Smith, D. S. Goodman, I. Sivarajah, J. E. Wells, S. Banerjee, R. Cote, H. H. Michels, J. A. M. Jr., and F. A. Narducci, Appl. Phys. B **114**, 75 (2014).
  - [16] H. Frst, T. Feldker, N. V. Ewald, J. Joger, M. Tomza, and R. Gerritsma, Phys. Rev. A **98**, 012713 (2018).
  - [17] Y.-Y. Jau, J. D. Hunker, and P. D. D. Schwindt, AIP. Adv. **5**, 117209 (2015).
  - [18] B. S. Mathur, H. Y. Tang, and W. Happer, Phys. Rev. A **2**, 648 (1970).
  - [19] W. Happer, Y.-Y. Jau, and T. Walker, *Optically Pumped Atoms* (Wiley-VCH, 2010).
  - [20] F. G. Major and H. G. Dehmelt, Phys. Rev. **170**, 91 (1968).
  - [21] T. V. Tscherbul, P. Brumer, and A. A. Buchachenko, Phys. Rev. Lett. **117**, 143201 (2016).
  - [22] S. Kadlecek, T. Walker, D. K. Walter, C. Erickson, and W. Happer, Phys. Rev. A **63**, 052717 (2001).